PERGAMON

International Journal of Heat and Mass Transfer 43 (2000) 2779–2791

International Journal of HEAT and MASS TRANSFER

www.elsevier.com/locate/ijhmt

Heat and mass transfer during drying of granular products — simulation with convective and conductive boundary conditions

A. Mhimid [a,*], S. Ben Nasrallah [a], J.P. Fohr [b]

[a] *Ecole Nationale d'Ingénieurs de Monastir, 5000 Monastir, Tunisia*
[b] *Laboratoire d'Etudes Thermiques, 40 Avenue du recteur Pineau, 86022 Poitiers, France*

Received 20 December 1996; received in revised form 20 June 1999

Abstract

Numerical simulation of grain drying in a vertical cylindrical bed has been carried out with specific boundary conditions: evaporation, which occurs with forced air flowing through the bed, is intensified with a conductive heat flux from the wall. We consider two mathematical models of heat and mass transfer through granular medium: two temperature model (No Local Temperature Equilibrium Model: NLTEModel) and one temperature model (Local Temperature Equilibrium Model: LTEModel). The air–grain mass transfer is expressed with a drying rate equation outcome from experiments. The resolution of the equations set is carried out, using a finite volume method. Different effects, such as the effect of the porosity variation on energy and mass transport, are discussed. Sensitivity to external conditions is determined. Finally, validity of local thermal assumption is examined.

1. Introduction

Drying of grains is an operation of great interest in the industrial and agricultural sectors. The optimization of the cost of this operation and the preservation of the quality require a study of heat and mass transfer during drying. Considerable work has been done, in the past decades on the development of theory and mathematical models for grains drying. Comprehensive reviews of these models and simulation methods are available in the literature [1–6].

In many granular medium models of flow, the principal hypotheses used by the authors are:

- the medium is at local thermal equilibrium;
- the two-dimensional effect is negligible;
- the effect of porosity variation is negligible.

To our knowledge, the validity of these hypotheses is not yet completely studied.

In this paper, we consider here the case of a static bed (cylinder bin) with two drying factors: a forced convective air flow through the bed (axial flow) and a heat flux from the lateral wall (Fig. 1). This process that can be encountered in storing silos where external walls are submitted to solar energy, is not studied.

The model used here is adapted from the general porous medium theory of Whitaker [7]. The air–grain mass transfer is described with a kinetic equation based on experimental data, which expresses the evaporation (or condensation) flow rate in relation to the characteristics of air and the state of grain along the drying. The solution of the system of the presented

* Corresponding author.

0017-9310/00/$ - see front matter
PII: S0017-9310(99)00286-0

Nomenclature

C_p	specific heat (J kg^{-1} K^{-1})
D_e	diffusion coefficient (m^2 s^{-1})
d_p	mean particle diameter (m)
h_{gs}	heat transfer coefficient between solid and gas (W m^{-2} K^{-1})
h_s	heat transfer coefficient between solid and the ambience (W m^{-2} K^{-1})
h_0	heat transfer coefficient at the entrance (W m^{-2} K^{-1})
L	height of the bed (m)
$\dot{m}$	evaporation rate (kg m^{-3} s^{-1})
P	pressure (Pa)
Pr	Prandtl number
q	heating flux (W m^{-2})
R	ray of the bed drying (m)
Re	Reynolds number
r	radial coordinate (m)
r^*	radial adimensional coordinate ($r^*=r/R$)
S	lateral area (m^2)
T	temperature (K)
T_{wb}	wet bulb temperature (K)
T^*	dimensionless temperature ($T^*=T-T_i/\Delta T_{ref}$)
t	time (s)
t^*	dimensionless time ($t^*=t/\tau$)
V_g	gas velocity (m s^{-1})
W	absolute humidity of air
X	moisture content (kg per kg of solid)
X^*	relative moisture content ($X^*=X/X_i$)
z	axial coordinate (m)
z^*	axial adimensional coordinate ($z^*=z/L$)

Greek symbols

ΔH	latent heat of evaporation (J kg^{-1})
Δr	depth increment (m)
Δz	depth increment (m)
Δt	time increment (s)
ε	bed porosity
λ	thermal conductivity (W m^{-1} K^{-1})
λ^*	effective thermal conductivity (W m^{-1} K^{-1})
ρ	density (kg m^{-3})
ϕ	humidity
τ	drying time (s) ($\tau=((1-\varepsilon)\rho_s\Delta X/\rho_a V_g\Delta W)L$ when the wall is adiabatic)
μ	dynamic viscosity (kg m^{-1} s^{-1})
ω	volume (m^3)
ξ	solid–gas transfer area (m^2 m^{-3})

Subscripts

a	air
cr	critical
eq	equilibrium
g	gas
i	initial
m, n	spatial index
s	solid
sat	saturation
v	vapor
wb	wet bulb

equations has been solved numerically by the finite volume method [8].

The time and space evolutions of the states variables are presented and analyzed. The sensitivity to external conditions is determined and the validity of the local thermal equilibrium assumption is examined.

2. Analysis

The problem under investigation is forced convection of the air through a vertical cylindrical packed bed (Fig. 1) of wet porous particles. The medium is discontinuous. The macroscopic equations, which govern heat and mass transfer, are generally obtained by changing the scale [7,9,10]. One passes from the microscopic view, in which the averaging volume is small compared to the pores, to the macroscopic view in which the averaging volume is large with regard to the pores. This scale changing enables us to convert the real discontinuous medium to a fictious continuous equivalent one. Each macroscopic term is obtained by averaging the microscopic one. The macroscopic differential equations are obtained by taking the average of the microscopic equations over the averaging volume, which holds a lot of grains, and by using closing assumptions. The microscopic equations are the equations of momentum, mass and energy conservation in all considered phases and at the interfaces. These equations are obtained by using thermodynamic and mechanic laws of continuous media.

Several assumptions are made in order to obtain a closed set of governing equations at macroscopic scale:

- the porous medium is homogeneous and isotropic;
- the porous particles are incompressible;
- the compression work and viscous dissipation are negligible;
- the inter-particle radiation heat transfer is neglected;
- the dispersion terms and the tortuosity terms can be modeled as diffusive fluxes;

- the forced convection dominates the packed bed, i.e. natural convection is negligible;
- the air velocity is constant ($\vec{V}_g = V_g\vec{e}_z$);
- the axial vapor diffusion in air and the counter diffusion for air are taken negligible;
- the axial conductive heat flux in the gas is negligible before the convective one.

2.1. Governing equations

When the transfers are two dimensional and depend on the r and z axes, the governing equations become:

2.1.1. Vapor mass conservation equation

$$\varepsilon\frac{\partial\rho_v}{\partial t} + \frac{\partial}{\partial z}(\rho_v V_g) = \dot{m} + +\frac{1}{r}\frac{\partial}{\partial r}\left[r\rho_g D_e \frac{\partial}{\partial r}\left(\frac{\rho_v}{\rho_g}\right)\right] \quad (1)$$

where D_e is the effective diffusivity. In the radial direction D_e has the following expression [11]:

$$D_e = 0.7D + 0.01DPe^{0.9} \quad (2)$$

D is the molecular diffusion of vapor in air and Pe is the Peclet number:

$$Pe = \frac{d_p V_g}{D}$$

d_p is the averaging grains diameter and V_g the velocity.

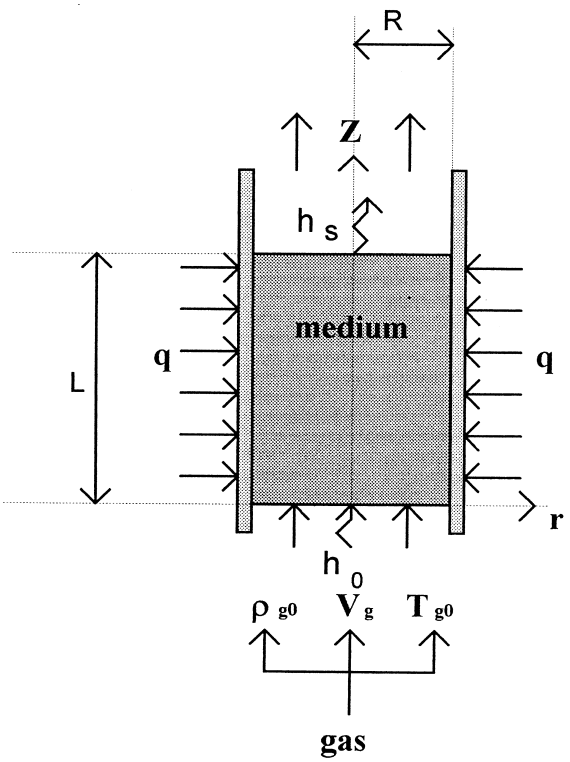

Fig. 1. Sketch of the fixed bed.

2.1.2. Air mass conservation equation

$$\varepsilon\frac{\partial\rho_a}{\partial t} + \frac{\partial(\rho_a V_g)}{\partial z} = 0 \quad (3)$$

The air and vapor density are tied with ideal gas equations as:

$$P_v = \rho_v\frac{R}{M_v}T_g; \quad P_a = \rho_a\frac{R}{M_a}T_g \quad (4)$$

Partial pressure P_a and P_v are part of the total pressure P:

$$P = P_a + P_v \quad (5)$$

2.1.3. Gas energy equation

$$\begin{aligned}&\varepsilon\rho_g C_{pg}\frac{\partial}{\partial t}(T_g) + \rho_g C_{pg} V_g \frac{\partial}{\partial z}(T_g)\\ &\quad = h_{gs}\xi(T_s - T_g) + \dot{m}C_{pv}(T_s - T_g)\\ &\qquad + \frac{1}{r}\frac{\partial}{\partial r}\left[r\varepsilon\lambda_{ge}\frac{\partial}{\partial r}(T_g)\right]\end{aligned} \quad (6)$$

The thermal dispersion effect was treated as a diffusive component added to the gas effective thermal conductivity [12]:

$$\varepsilon\lambda_{ge} = \varepsilon\lambda_g + 0.1Pr\left(\frac{\rho_g V_g d_p}{\mu_g}\right)\lambda_g \quad (7)$$

2.1.4. Solid energy equation

$$\begin{aligned}&(1-\varepsilon)\rho_s(C_{ps} + XC_{pe})\frac{\partial T_s}{\partial t}\\ &\quad = h_{gs}\xi(T_g - T_s) - \dot{m}\Delta H_{vap} + \frac{\partial}{\partial z}\left[(1-\varepsilon)\lambda_{se}\frac{\partial T_s}{\partial z}\right]\\ &\qquad + \frac{1}{r}\frac{\partial}{\partial r}\left[(1-\varepsilon)r\lambda_{se}\frac{\partial T_s}{\partial r}\right]\end{aligned} \quad (8)$$

where $\dot{m}$ is the evaporation rate and ΔH_{vap} is the latent heat of vaporization.

$$\Delta H_{vap} = H_v(T_s) - H_e(T_s)$$
$$= \Delta H^0_{vap} + (C_{pv} - C_{pe})T_s \quad (9)$$

T_s and T_g are the average intrinsic temperatures of the solid and the gas, respectively. λ_{se} and λ_{ge} are the effective thermal conductivities of the solid and the gas. ρ_a, ρ_v, ρ_g and ρ_s are, respectively, the average intrinsic densities of the air, vapor, gas and solid phases. C_{pa}, C_{pv}, C_{pg} and C_{ps} are the specific heats of the air, vapor, gas and solid, respectively. H_{gs} and ξ are the heat transfer coefficient and the solid–gas transfer area, respectively. D_e and ε are the effective diffusivity and the bed porosity, respectively. V_g is the gas velocity.

The specific surface area of the packed bed, which appears in the energy equations, is [13]:

$$\xi = \frac{6(1-\varepsilon)}{d_p} \quad (10)$$

The heat transfer coefficient between solid and gas is given by [14]:

$$h_{gs} = \frac{\lambda_g}{d_p}(2 + 1.8Pr^{0.33}Re^{0.5}) \quad (11)$$

Pr is the Prandtl number and *Re* is the Reynolds number.

2.1.5. Energy equation when LTE is valid

One of the assumptions made in many studies consists in considering T_g equal to T_s at any point (the medium is considering at local thermal equilibrium LTE). Then, a single equation is sufficient to determine the temperature field in the dryer. To avoid transfer terms, this equation is obtained by adding Eqs. (6) and (8).

$$[(1-\varepsilon)\rho_s(C_{ps} + XC_{pe}) + \varepsilon\rho_g C_{pg})]\frac{\partial T}{\partial t} + \rho_g C_{pg} V_g \frac{\partial T}{\partial z}$$
$$= -\dot{m}\Delta H_{vap} + \frac{\partial}{\partial z}\left[(1-\varepsilon)\lambda_{se}\frac{\partial T}{\partial z}\right] + \frac{1}{r}\frac{\partial T}{\partial r}\left[r\lambda^*\frac{\partial T}{\partial r}\right] \quad (12)$$

where $\lambda^* = (1-\varepsilon)\lambda_{se} + \varepsilon\lambda_{ge}$.

The model formed by Eqs. (1), (3), (6) and (8) on one hand and by Eqs. (1), (3) and (12) on the other hand will be denoted in the continuation of this paper as NLTEModel and LTEModel, respectively.

2.1.6. Porosity variation

In most theoretical and numerical studies the variations of the bed porosity were approximated by an exponential function of the form [18,19]:

$$\varepsilon = \varepsilon_0\left(1 + C\ \exp\left(-N\frac{r}{d_p}\right)\right) \quad (13)$$

where d_p is the particle diameter, C and N are empirical constants chosen so that the porosity approaches unity near the wall while it decreases to ε_0 about four particle diameters away from the wall.

2.1.7. Kinetic equation

The mass rate of evaporation (or condensation) is:

$$\dot{m} = -(1-\varepsilon)\rho_s\frac{\partial X}{\partial t} = -(1-\varepsilon)\rho_s\dot{X} \quad (14)$$

where $\dot{X}$ is dependent on the moisture content X, the gas temperature T_g, the absolute gas humidity W and the gas velocity V_g. Van Meel [15] proposed a standard drying curve as:

$$\frac{\dot{X}}{\dot{X}_{in}} f(X_+); \quad X_+ = \frac{X - X_{eq}}{X_{cr} - X_{eq}} \quad (15)$$

X_{cr} is the critical moisture content indicating the start of the period of decreasing drying rate period. X_{cr} depends on the initial drying rate $\dot{X}_{in}$, the body thickness, as well as other factors such as the temperature and internal structure of the material.

X_{eq} is the equilibrium grain moisture. X_{eq} depends on the gas humidity and temperature. The form of the drying rate proposed by Van Meel [15] is adequate for products, which show a first period of constant drying rate $\dot{X}_{in}$. In this case the grain surface remains saturated at a temperature equal to the wet bulb temperature. Most of biological products do not present such an initial period and $\dot{X}_{in}$ is taken as the initial drying rate.

The drying rate equation used in this study is deduced from Muhlbauer's results [16] for corn:

$$f(X_+) = 1 \quad \text{when } X_+ > 1,$$

$$f(X_+) = a_1X_+ + a_2X_+^2 + a_3X_+^3 \quad \text{when } X_+ < 1 \quad (16)$$

where $a_1 = 0.97 - 0.0018T_g$, $a_2 = -3.73 + 0.0022T_g$, $a_3 = 3.76 + 0.002T_g$

$$\dot{X}_{in} = X_{in}V_g^{0.5}[W_{sat}(T_s) - W]f(T_s) \quad (17)$$

where $W = \rho_v/\rho_a$, and $X_{cr} = 0.8X_{in}$. $f(T_s)$ is a correction function given by:

$$f(T_s) = [0.1619T_s - 2.427]10^{-3} \quad \text{if } T_s < 353\ \text{K}$$

$$f(T_s) = [0.2328T_s - 8.102]10^{-3} \quad \text{if } T_s > 353\ \text{K}$$

For corn, the moisture content at equilibrium X_{eq} is given by the following expression [17]

$$X_{eq} = [61 \times 10^{-5} + 0.685\phi - 1.202\phi^2 + 0.888\phi^3] \exp\left[-\frac{T_g}{100}\right] \quad (18)$$

where ϕ is the relative humidity ($\phi = \rho_v/\rho_{vsat}(T_g)$).

2.2. Boundary and initial conditions

2.2.1. Initial conditions

Initially, temperatures, gas densities and moisture contents are constant:

$$T_s(0, r, z) = T_g(0, r, z) = T_i$$

$$\rho_v(0, r, z) = \rho_{vi}$$

$$\rho_a(0, r, z) = \rho_{ai}$$

$$X(0, r, z) = X_i$$

2.2.2. Densities boundary conditions

At the inlet of the bed ($z = 0$) the density of air and of vapor are assumed constant:

$$\rho_v(t, r, 0) = \rho_{v0}; \quad \rho_a(t, r, 0) = \rho_{a0} \quad (19)$$

The lateral heated area is impervious, thus:

$$\frac{\partial}{\partial r}(\rho_v)(t, R, z) = 0; \quad \frac{\partial}{\partial r}(\rho_a)(t, R, z) = 0 \quad (20)$$

Taking into account the symmetry about the z axis, we can write:

$$\frac{\partial}{\partial r}(\rho_v)(t, 0, z) = 0; \quad \frac{\partial}{\partial r}(\rho_a)(t, 0, z) = 0 \quad (21)$$

2.2.3. Thermal boundaries conditions for the NLTEModel

At the inlet ($z = 0$) the temperature of the gas is assumed constant:

$$T_g(t, r, 0) = T_{g0}$$

The solid and gas temperatures are related by:

$$\lambda_{se}\frac{\partial T_s}{\partial z}(t, r, 0) = h_0(T_s - T_g) \quad (22)$$

At the outlet of the cylindrical bed ($z = L$), the transfers are not well known and the flow existing on the porous surface is very complex. In order to solve this problem correctly, it is necessary to extend the domain of computation to take into account the flow and the heat transfer in the fluid near the upper surface, which may complicate enormously this study. To avoid this problem we have introduced a heat transfer coefficient h_s:

$$-\lambda_{se}\frac{\partial T_s}{\partial z}(t, r, L) = h_s(T_s - T_a) \quad (23)$$

The lateral area ($r = R$) is heated at a constant heating flux. Each of the individual phases at the wall surface will receive the same heat flux density q [11,20,21]. We can write:

$$-\lambda_{se}\frac{\partial T_s}{\partial r}(t, R, z) = q; \quad -\lambda_{ge}\frac{\partial T_g}{\partial r}(t, R, z) = q \quad (24)$$

Taking into account the symmetry about the z axis, we deduce that:

$$-\lambda_{se}\frac{\partial T_s}{\partial r}(t, 0, z) = 0; \quad -\lambda_{ge}\frac{\partial T_g}{\partial r}(t, 0, z) = 0 \quad (25)$$

2.2.4. Thermal boundaries conditions for the LTEModel

Initially, the temperature is uniform: $T(0, r, z) = T_i$

At the inlet ($z = 0$) we have:

$$\lambda_{se}\frac{\partial T}{\partial z}(t, r, 0) = h_0(T - T_0) \quad (26)$$

At the outlet of the cylinder ($z = L$), considering T_g equal to T_s we obtain:

$$-\lambda_{se}\frac{\partial T}{\partial z}(t, r, L) = h_s(T - T_a) \quad (27)$$

At the lateral area ($r = R$) we have also:

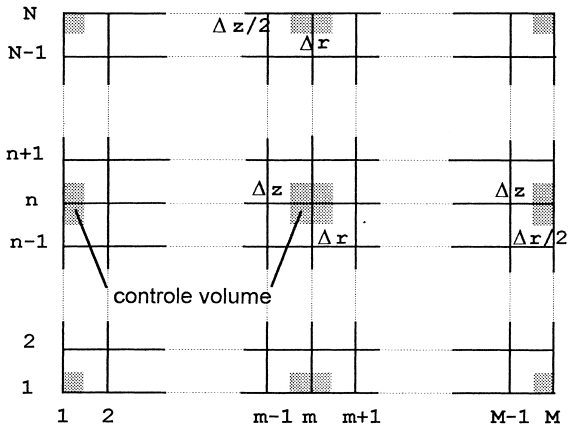

Fig. 2. Numerical grid.

$$-\lambda^* \frac{\partial T}{\partial r}(t, R, z) = q \tag{28}$$

Taking into account the symmetry about the z axis, we deduce that:

$$-\lambda^* \frac{\partial T}{\partial r}(t, 0, z) = 0 \tag{29}$$

3. Numerical solution

The system of the presented equations is solved numerically by the method of control volume as described by Patankar [8]. The advantage of this method is that it ensures flux conservation, and thus avoids generation of parasitic sources. The method consists of defining a grid of points $P_{n,m}$ within the calculated domain and then constructing around each point a control volume (Fig. 2). The value of a physical quantity ψ at any point $P_{n,m}$ and at the time $t+\Delta t$ will be noted $\psi_{n,m}^{i+1}$. The equations are integrated over this control domain over an interval of time $[t, t+\Delta t]$.

In order to discretize the resulting integral equations back to algebraic equations tying together the solution values at the nodes of the grid, we make the following hypotheses:

- the fluxes are constant on the face of the control volume which is perpendicular to them;
- the accumulation terms and the source terms can be approximated by averages on the control volume constructed around $P_{n,m}$.

To avoid numerical instabilities we adopted an implicit scheme.

At the boundaries of the bed, the equations are discretized by integration over half the control volume and by taking into account the boundary conditions. At the corner we used a quarter of the control volume.

The terms of transport by convection are discretized using an upwind scheme. This scheme assumes that the values of the conserved quantities at the face of the control volume are equal to their values at the grid point situated upstream.

The first derivatives, which are evaluated on the control volume faces, are approximated over two nodes within the porous medium.

$$\left[\frac{\partial \Psi}{\partial z}\right]_{n+1/2,\,m}^{i+1} = \frac{\Psi_{n+1,\,m}^{i+1} - \Psi_{n,\,m}^{i+1}}{\Delta z}$$

Considering these assumptions, the general form of the resulting algebraic equations becomes:

$$A_0 \Psi_{n,\,m}^{i+1} = A_{\mathrm{w}} \Psi_{n,\,m-1}^{i+1} + A_{\mathrm{e}} \Psi_{n,\,m+1}^{i+1} + A_{\mathrm{s}} \Psi_{n-1,\,m}^{i+1} + A_{\mathrm{n}} \Psi_{n+1,\,m}^{i+1} + A_1$$

The resulting system of algebraic equation is solved numerically by the iterative line-by-line sweeping method. The choice of this method is justified by its rapidity of convergence compared to point by point methods. Scanning along the r axis, we set:

$$A_0 \Psi_{n,\,m}^{i+1} = A_{\mathrm{w}} \Psi_{n,\,m-1}^{i+1} + A_{\mathrm{e}} \Psi_{n,\,m+1}^{i+1} + D$$

where

$$D = A_{\mathrm{s}} \Psi_{n-1,\,m}^{i+1} + A_{\mathrm{n}} \Psi_{n+1,\,m}^{i+1} + A_1$$

This solution method consists in the evaluation using the predicted solution of A_0, A_{w}, A_{e} and D. Then, the resulting tridiagonal system of equations is solved by the standard Gaussian-elimination method. If the difference between the calculated and estimated solutions is small, the convergence to the solution is achieved, or else we repeat the procedure for the evaluation of the coefficients using the solution already calculated until convergence is reached.

4. Numerical data

The cylinder is 0.50 m high and 0.10 m in radius. This cylinder is filled with grains and opened from both sides. It is crossed by an air flow which has, at the inlet, constant physical characteristics (temperature, humidity, and velocity). The cylinder lateral area is heated by a constant heat flux density q = 200 W m^{-2}

The physical characteristics of the medium (corn) and the gas are [4]: $\varepsilon = 0.4$, $d_{\mathrm{p}} = 4$ mm, $D_{\mathrm{e}} = 2 \times 10^{-4}$ $\mathrm{m}^2\ \mathrm{s}^{-1}$, $\rho_{\mathrm{s}} = 1260$ kg m^{-3}, $\lambda^* = 0.15$ W $\mathrm{m}^{-1}\ \mathrm{K}^{-1}$, $\varepsilon\lambda_{\mathrm{ge}} = 0.05$ W $\mathrm{m}^{-1}\ \mathrm{K}^{-1}$, $(1-\varepsilon)\lambda_{\mathrm{se}} = 0.10$ W $\mathrm{m}^{-1}\ \mathrm{K}^{-1}$, $C_{\mathrm{ps}} = 1463$ J $\mathrm{kg}^{-1}\ \mathrm{K}^{-1}$ and $C_{\mathrm{pg}} = 1560$ J $\mathrm{kg}^{-1}\ \mathrm{K}^{-1}$. The initial conditions are: $T_{\mathrm{si}} = T_{\mathrm{gi}} = 290$ K (17°C), $W_{\mathrm{i}} = 0.0125$ and $X_{\mathrm{i}} = 0.67$ kg of water/kg of solid. The characteristics of inlet air flow are: $V_{\mathrm{g}} = 0.1$ m s^{-1}, $T_{\mathrm{g0}} = 323$ K (50°C), $W_0 = \rho_{\mathrm{v0}}/\rho_{\mathrm{a0}} = 0.0074$ and $T_{\mathrm{a}} = 17$°C. The characteristic values of variables, used later are: $\tau = L/C$ is a drying characteristic time. C is the celerity of the drying front defined, when the wall is adiabatic [3], as:

$$C = \frac{V_{\mathrm{g}} \rho_{\mathrm{a}}}{(1-\varepsilon)\rho_{\mathrm{a}}} \frac{\Delta W}{\Delta X}$$

where

$$\Delta X = X_{in} - X_{eq}, \quad \Delta W = W_{sat}(T_{wb}) - W_0$$

The heat flux used for the drying is issued partly from lateral wall and partly by air flow. α is the applied heat fluxes ratio defined by:

$$\alpha = \frac{qS}{\pi R^2 \rho_{g0} V_g C_{pg} \Delta T_{ref}}$$

where $S = 2\pi RL$ and $\Delta T_{ref} = T_0 - T_{wb}(T_0, W_0)$, T_{wb} is the wet bulb temperature obtained from T_0 and W_0 through moist air chart. $T_a = 290$ K (17°C), $\Delta T_{ref} = 27$°C, $\Delta X = 0.60$ kg of water/kg of solid and, $\Delta W = 0.0105$ kg of water/ kg of air.

The sensitivity of coupled heat and mass transfer in the porous bed to heat and mass transfer coefficients has been studied [20]. In the present study, we have taken the following values: $h_0 = h_s = h_g = 20$ W m^{-2} K^{-1}.

5. Results and discussion

5.1. Validation of the numerical simulation

The numerical simulation has been validated by comparison with experimental global kinetic

$$\frac{\dot{\bar{X}}}{(T_g - T_{wb})\sqrt{V_g}} = f(X)$$

for a thin bed obtained by Fornell published in Ref. [22]. The numerical simulation is made by taking the same conditions as those of the experiment ($V_g = 0.85$ m s^{-1}, $T_{g0} = 333$ K, and $T_{wb} = 299$ K). Fig. 3 shows that the experimental and the numerical model results are identical.

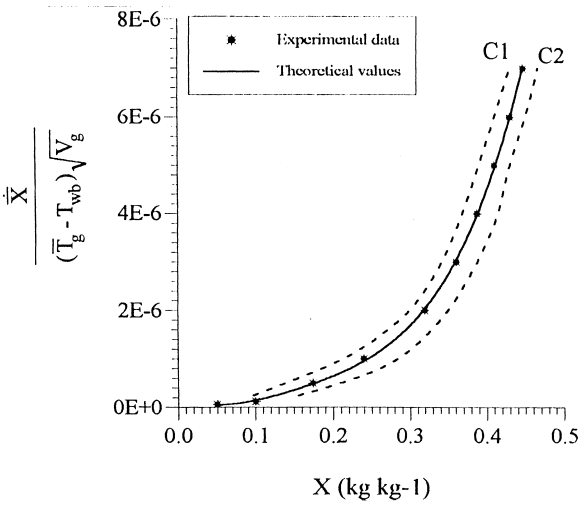

Fig. 3. Experimental and calculated drying kinetics: all curves of drying kinetics obtained by Fornell (1978) are situation between C_1 and C_2 ($\bar{X}(=1/\omega)\int_\omega X\,d\omega$ $\bar{T}_g(=1/\omega)\int_\omega T_g\,d\omega$, $0.85 < V_g < 1.8$ m s^{-1}, $60 < T_{g0} < 100$°C, $26 < T_{wb} < 38$).

As far as we know, there are no experimental measures for thick corn beds. Yet this does not hinder a theoretical study of heat and mass transfers from a thick corn bed and so as to optimize the dryer.

5.2. General description

The results of the numerical simulation are presented as a curve giving the spatial evolution of the relative solid temperature (Fig. 4), and the relative moisture content (Fig. 5) at different times ($t^* = 5.5 \times 10^{-5}$, $t^* = 3.2 \times 10^{-3}$, $t^* = 0.039$, $t^* = 0.098$, $t^* = 0.196$, and $t^* = 0.816$, where t^* is the dimensionless time).

In these figures, we can see a front of evaporation that moves with time and divides the bed in two regions (dried region and wet region) (Fig. 5). Evaporation is essentially localized in the zone in which the gradient of moisture content is high (front of evaporation). The obtained results show that the region close to the wall is rapidly dried. When time increases the front of evaporation approaches the outlet of the medium and the humid region contracts.

The numerical simulation shows that the grains overheat at the inlet and near the heated surface (Fig. 4). When time increases, the overheating propagates inside the medium. The solid temperature, under the chosen conditions, does not decrease from its initial value in the medium (the initial temperature T_i is less than the wet bulb temperature T_{wb}). At the end of drying, the solid temperature and the moisture content tend to their final values in all the medium, and the evaporation ceases.

We can notice that when the air velocity and the inlet temperature increase, the front evaporation moves more quickly and, consequently the time necessary for drying decreases (Figs. 6 and 7).

Fig. 8 shows the time space evolution of the relative difference temperature

$$\Delta T_s^* = \left| \frac{T_g - T_s}{\Delta T_{ref}} \right|$$

between solid temperature and gas temperature calculated during drying with the NLTEModel. At the beginning, this difference is only important at the inlet of the bed, because the inlet temperature is higher than the initial medium temperature. After that there is a difference only near the lateral area and in region where the front evaporation is localized. This difference is due to the difference between the thermal characteristics of the solid and the gas. As has been reported previously [23,24], the difference

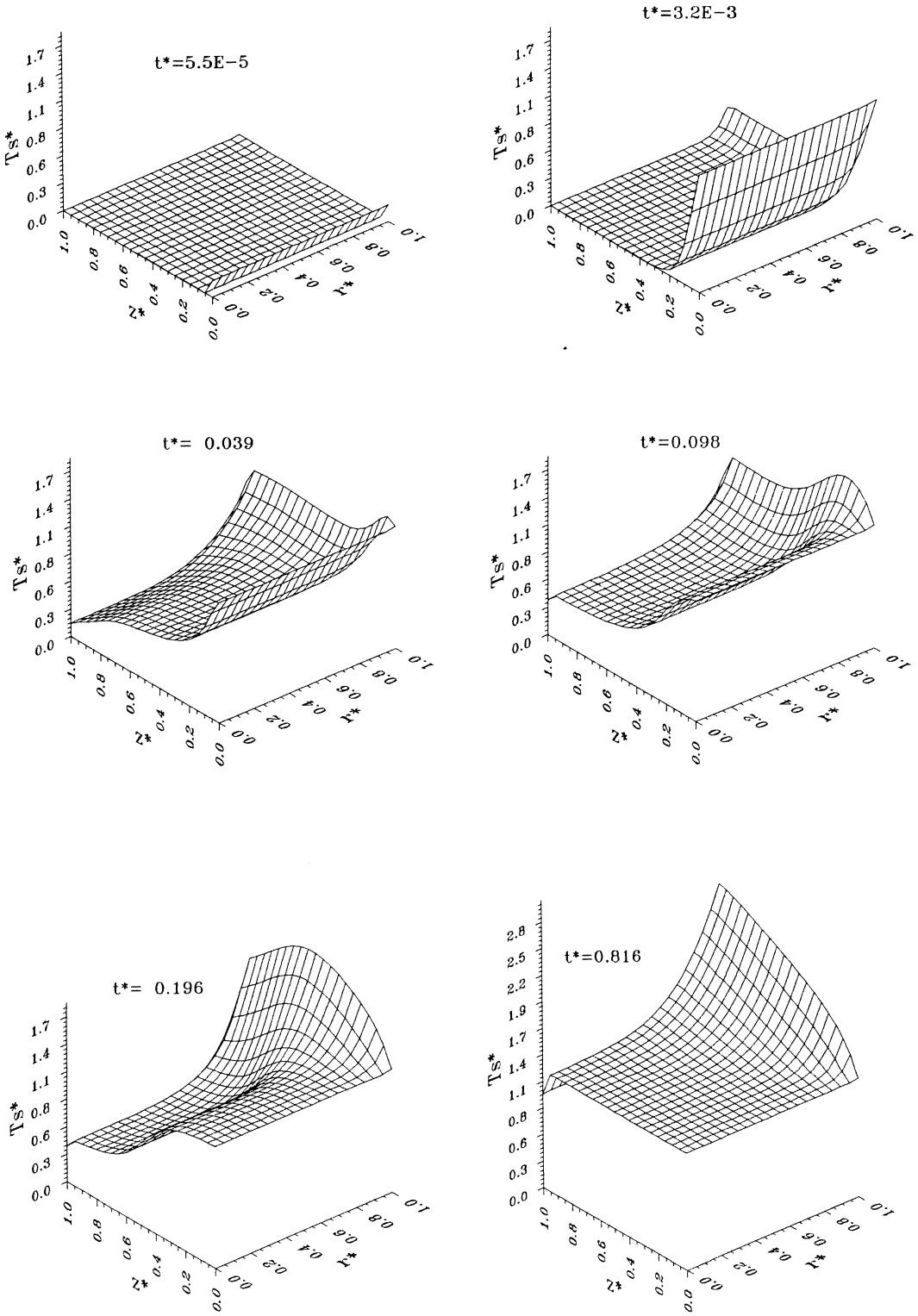

Fig. 4. Time–space evolution of the relative solid temperature calculated by NLTEModel ($T_s^* = (T_s - T_{wb}/T_0 - T_{wb})$, $V_g = 0.1$ m s^{-1}, $q = 200$ W m^{-2}).

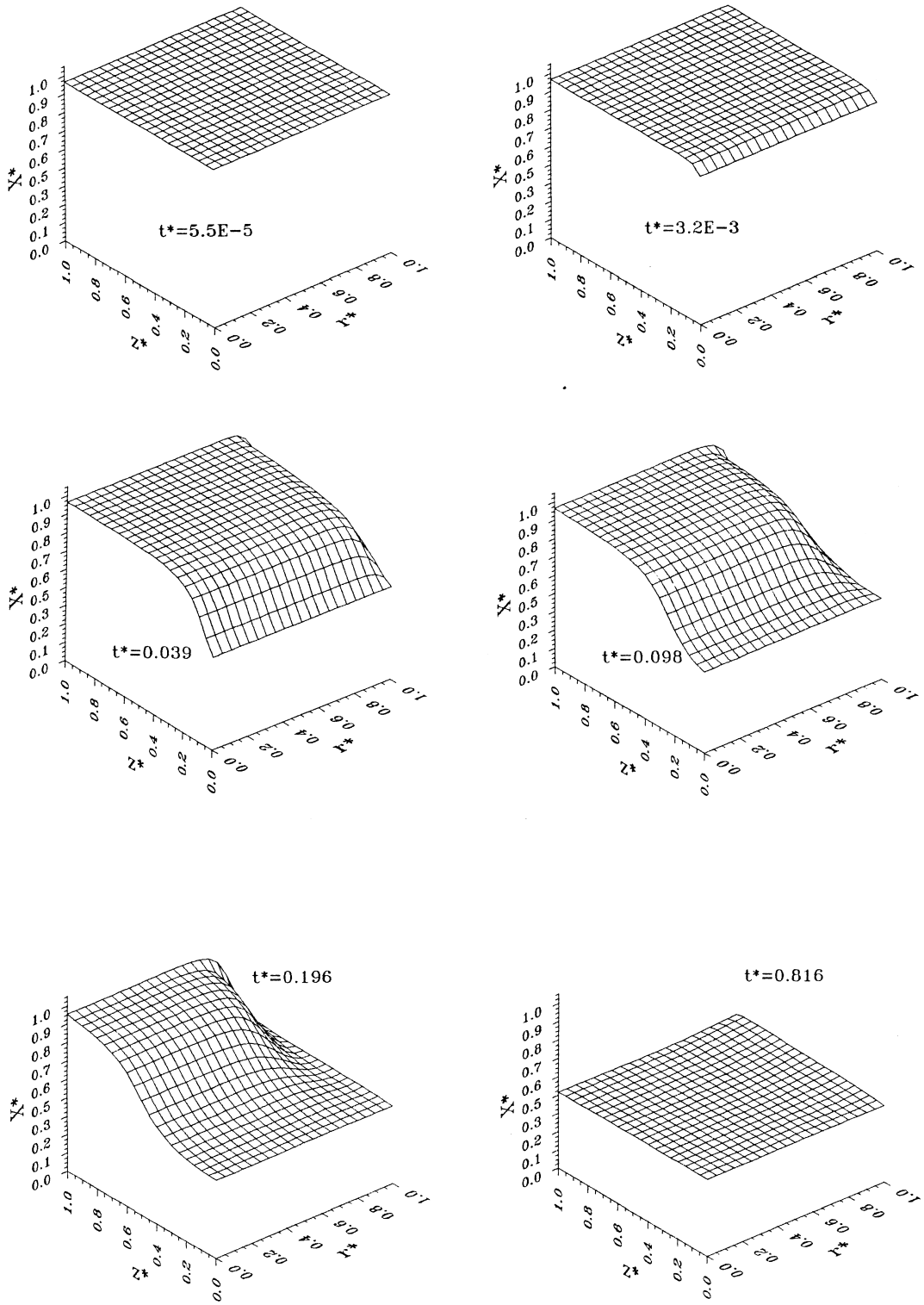

Fig. 5. Time–space evolution of the relative moisture content calculated by NLTEModel ($X^* = X/X_i$, $V_g = 0.1$ m s^{-1}, q = 200 W m^{-2}).

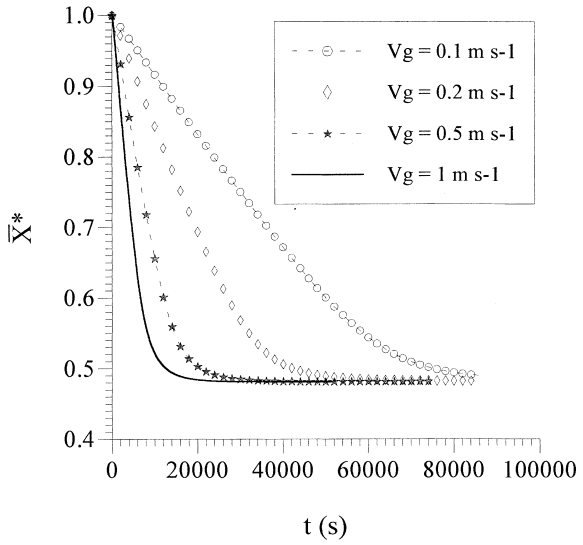

Fig. 6. Influence of the velocity on the total relative moisture content ($\bar{X}^* = \bar{X}/X_i = 1/\omega \int_\omega X/X_i \, d\omega$).

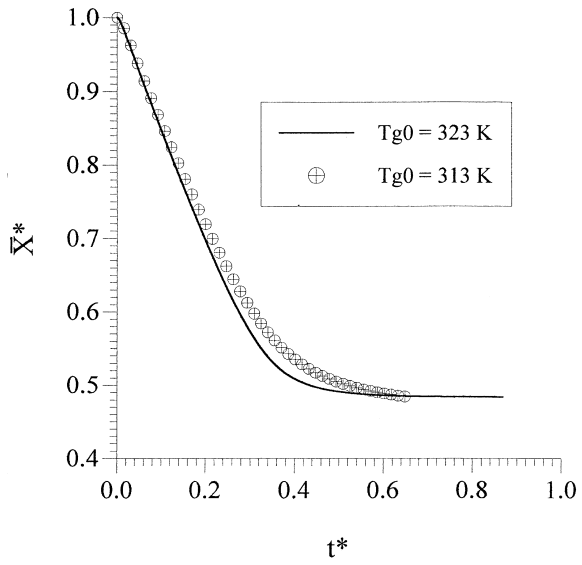

Fig. 7. Influence of the inlet temperature on the total relative moisture content.

$$\Delta T_s^* = \left| \frac{T_g - T_s}{\Delta T_{ref}} \right|$$

depends essentially on the $\lambda_{se}/\lambda_{ge}$ and decreases when this ratio tends to unity.

After a large time this difference appears at the outlet of the bed. We have observed that, the relative values of the temperature difference are less than 2.4% in the whole medium (see Table 1).

5.3. Effect of applied heat fluxes ratio

Convective heat transfer is inherent in the problem since velocity and temperature are imposed at the entrance conditions. In addition, a wall heat flux is imposed to simulate external conditions such as solar irradiation. This wall flux increases the drying rate near the wall and therefore decreases the drying time (see Fig. 9). When the ratio $\alpha = 0$, our results agree well with the predictions of the adiabatic wall [3].

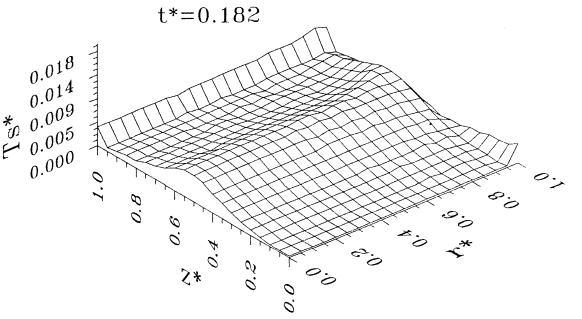

Fig. 8. Time–space evolution of the relative difference between solid and gas temperature ($\Delta \bar{T}_s^* = | (T_g - T_s/\Delta T_{ref}) |$, $V_g = 0.1$ m s^{-1}, $q = 200$ W m^{-2}).

5.4. Effect of heat coefficients h_0 and h_s

The effect of the heat transfer coefficient h_s on the heat and mass transfer is localized only near the outlet

Table 1

t^*	max$\lvert(T_g - T_s/\Delta T_{ref})\rvert$ (%)	max$\lvert(T - T_s/\Delta T_{ref})\rvert$ (%)	max$\lvert(X_N - X/X_i)\rvert$ (%)
0.006	2.4	4	0.6
0.036	1.1	9	2.9
0.183	0.6	24.5	10.5
0.515	0.9	6.6	3.1
0.727	0.9	8	0.25

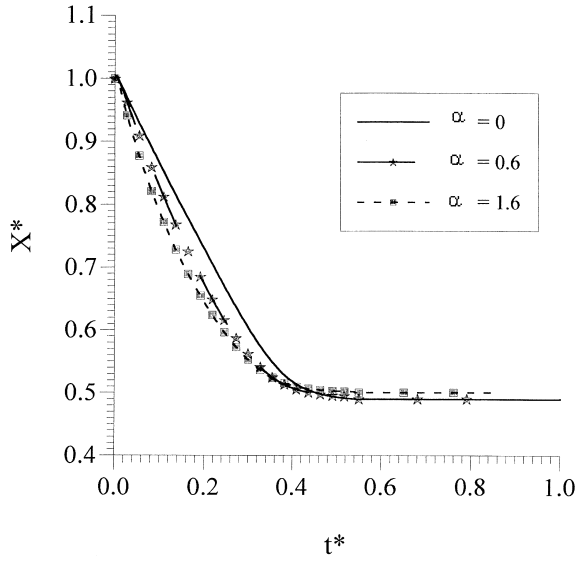

Fig. 9. Influence of the heat flux on the total relative moisture content ($\Delta T_{ref}=27°C$, $V_g=0.1$ m s^{-1}, q = 200 W m^{-2}).

of the bed and after a large drying time. The results are not sensitive to the inlet boundary conditions [20]. Consequently, the results of the total relative moisture content are identical when we have varied the values of heat coefficients h_0; we can notice that the difference between the results of the relative moisture content obtained for two values of the heat transfer coefficients h_s, appears only at the end of drying process (Fig. 10).

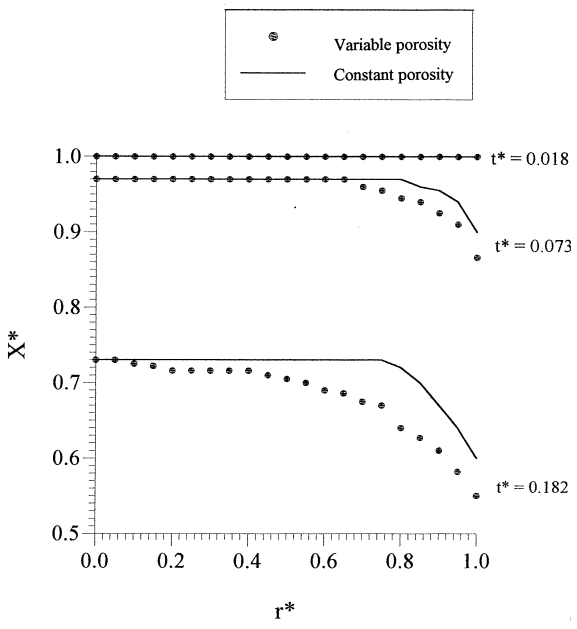

Fig. 11. Evolution of the moisture content $X^*(L/2, r)$ at different times. ($X^*=X/X_i$, $z^*=0.5$).

5.5. Porosity variation effects

The results show that the region close to the wall becomes dry faster when the bed porosity is variable (Fig. 11). This explains the difference between the values of the total moisture content obtained when the

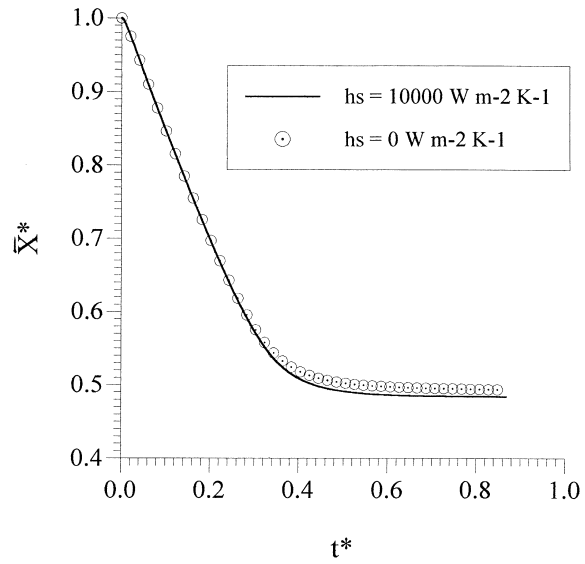

Fig. 10. Influence of the coefficient heat h_s on the total relative moisture content.

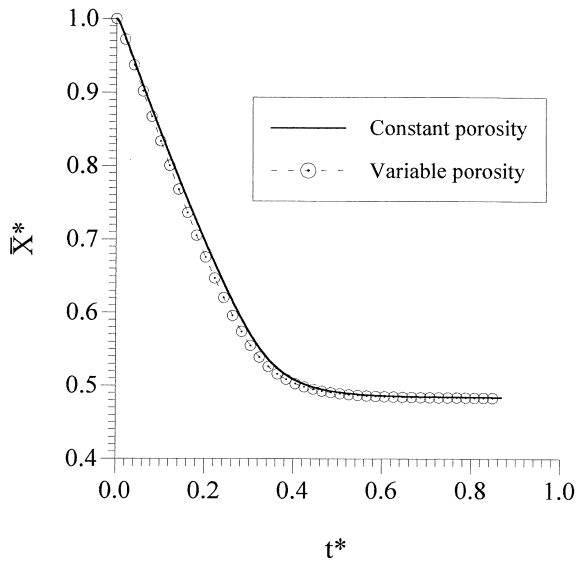

Fig. 12. Influence of the porosity variation on the total relative moisture content.

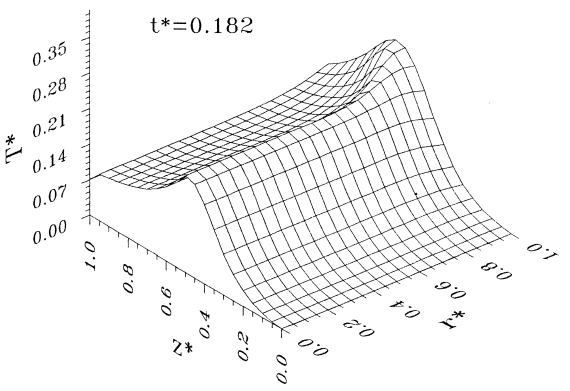

Fig. 13. Evolution of the relative difference between solid temperature T_s calculated by NLTEModel and temperature T calculated by LTEModel ($\Delta T^* = |(T - T_s/\Delta T_{ref})|$ $\alpha = 0.4$).

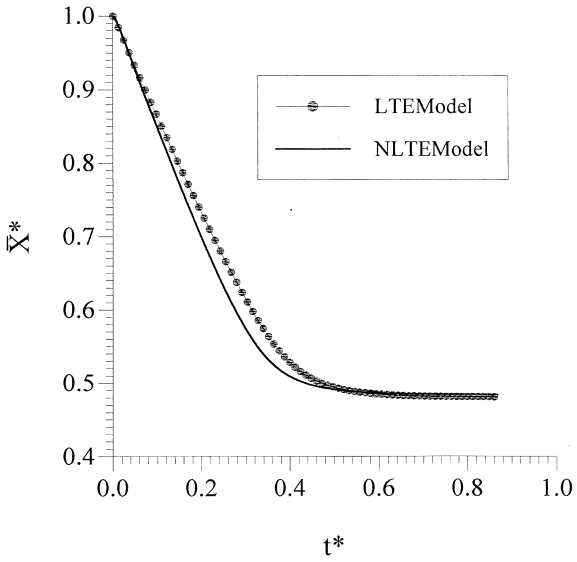

Fig. 15. Evolution of the total relative moisture content ($\alpha = 0.4$).

porosity is constant and when the porosity is variable (Fig. 12).

5.6. Comparison between LTEModel and NLTEModel results

The relative difference

$$\Delta T^* = \left| \frac{T - T_s}{\Delta T_{ref}} \right|$$

between the solid temperature T_s obtained by the NLTEModel and the temperature T obtained by the LTEModel has been compared (Fig. 13). At the beginning, there is a difference only important at the inlet of the bed. After that there is a difference near the lateral area and in region where the front evaporation is localized. At the end of drying, there is a difference only at the bed outlet. This difference is due to the fact that equilibrium pressure is very sensitive to temperature.

Fig. 14 shows the time space evolution of the difference of the relative moisture content calculated by the NLTEModel and by the LTEModel. We can notice that the results obtained by the two models are different at the region where the front evaporation takes place. Consequently, the total relative moisture content obtained by the two models plotted in Fig. 15 shows a difference during drying phenomena. At the end of drying, the total moisture content tends to the same value.

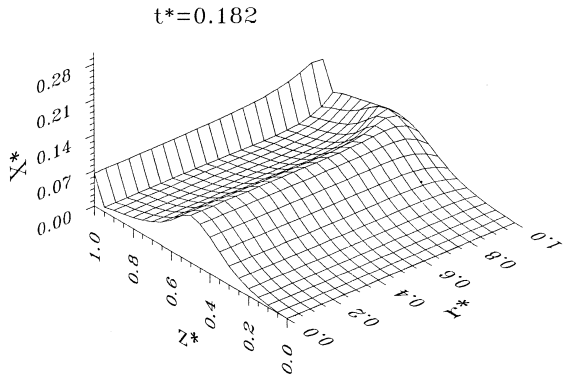

Fig. 14. Evolution of the relative difference between moisture content calculated by NLTEModel and moisture content calculated by LTEModel ($\Delta X^* = |(X_{NLTE} - X_{LTE}/X_i)|$ $\alpha = 0.4$).

6. Conclusions

A numerical simulation of convective/conductive drying in a cylindrical bed is undertaken. The heat and mass transfer model used in these calculations takes into considerations: either one or two temperature model; drying by forced convection and conductive heating at the wall, and higher porosity near the wall. The results reveal that complementary drying by wall heating is not efficient as convective heating. The higher porosity near the wall induces faster heating in this region. On the other hand, the two temperature model is not justified except in certain particular cases such as very high air velocities and fragile products of which one has to control perfectly the temperature at every instant.

References

[1] D.B. Brooker, F.W. Bakker-Arkema, C.W. Hall, Drying Cereal Grains, The Avi.

[2] J.R. Sharp, A review of low temperature drying simulation, J. Agric. Engng Res. 27 (1982) 169–190.

[3] G. Arnaud, J.-P. Fohr, Slow drying simulation in thick layers of granular products, Int. J. Heat Mass Transfer 31 (12) (1988) 2517–2526.

[4] J.P. Fohr, H. Ben Moussa, Heat and mass transfer in a cylindrical grain silo submitted to a periodical wall heat flux, Int. J. Heat Mass Transfer 37 (12) (1994) 1699–1712.

[5] P.L. Douglas, et al., Modeling and simulation of cross flow grain dryers — part I: model development, Trans. IChemE 72 (1994) 325–331 Part A.

[6] S. Sokhansanj, R.J. Gustafson, Prediction of heat and mass transfer within a drain kernel — a finite element application, in: A.S. Mujumdar (Ed.), Proceedings of Second International Drying Symposium, 1980, pp. 229–232.

[7] S. Whitaker, Simultaneous heat, mass and momentum transfers in porous media: a theory of drying, Advances of Heat Transfer 13 (1977) 119–203.

[8] S.V. Patankar, Numerical Heat Transfer and Fluid Flow, Publishing Corporation, McGraw-Hill Company, 1980.

[9] R.G. Carbonel, S. Whitaker, Heat and mass transfer in porous media, in: J. Bear, Corapcioglu (Eds.), Fundamentals of Transport Phenomena in Porous Media, Martinus Nijhoff Publishers, Netherlands, 1984, pp. 121–199.

[10] M. Quintard, S. Whitaker, One and two equation models for transient diffusion process in two phases systems, Advances of Heat Transfer 23 (1993) 369–464.

[11] M. Sahimi, Flow and Transport in Porous Media and Fractured Rock Printed in the Federal Republic of Germany, 1995.

[12] A. Amiri, K. Vafai, T.M. Kuzay, Effects of boundary conditions on non Darcian heat transfer through porous media and experimental comparisons, Numerical Heat Transfer 27 (1995) 651–664 Part A.

[13] K. Vafai, M. Sôzen, Analysis of energy and momentum transport for fluid flow through a porous bed, Int. J. Heat Mass Transfer 112 (1990) 690–699.

[14] W.E. Ranz, Friction and transfer coefficients for single particles and packed beds, Chemical Engineering Progress 48 (5) (1952) 247–253.

[15] Van Meel, Adiabatic convection batch drying with recirculation of air, Chem. Engng Sci. 9 (1958) 36.

[16] W. Muhlbauer, Recherches sur le séchage du mais-grain et étude d'un dispositif de séchage à co-courants, Traduction du CNEEMA, étude n°415, mai 1976.

[17] J.H. Rodriguez Arias, Desorptions isotherms and drying rate of shelled corn in the range of 40 to 140°F, PhD thesis, Department of Agricultural Engineering Michigan State University, 1956.

[18] A. Amiri, K. Vafai, Analysis of dispersion effects and non-thermal equilibrium, non Darcian, variable porosity incompressible flow through porous midia, Int. J. Heat Mass Transfer 37 (6) (1994) 939–954.

[19] P. Cheng, D. Vortmeyer, Transverse thermal dispersion and wall channeling in packed bed with forced convective flow, Chem. Engng Sci. 43 (9) (1988) 2523–2532.

[20] A. Mhimid, S. Ben Nasrallah, Theoretical study of heat and mass transfer during drying of granular products, in: Turner, Mujumdar (Eds.) Mathematical Modeling and Numerical Techniques in Drying Technology, New York, 1997, pp. 381–413 (Chapter 10).

[21] A. Mhimid, S. Ben Nasrallah, Heat and mass transfer during drying of granular products — simulation with convective and conductive boundary conditions, in: Proceedings of National Heat Conference, Baltimore, 10–12 August, 1997.

[22] J.J. Bimbenet, Le séchage dans les industries agricoles et alimentaires Cahiers de Génie Industriel Alimentaire, 4e cahier de GIA, Octobre, 1978.

[23] S. Ben Nasrallah, T. Amara, M.A. Dupeuty, Convection naturelle instantionnaire dans un cylindre rempli de grains ouvert a ses extrémités et dont la paroi est chauffée par un flux de chaleur constant: validité de l'hypothèse de l'équilibre thermique local, Int. J. Heat Mass Transfer 40 (5) (1997) 1155–1168.

[24] M. Combarnous, S. Bories, Hydrothermal convection in saturated porous media, Adv. Hydrosci. 10 (1975) 231–307.